Journal of Photochemistry and Photobiology A: Chemistry 209 (2010) 147–152

Contents lists available at ScienceDirect

Journal of Photochemistry and Photobiology A: Chemistry

journal homepage: www.elsevier.com/locate/jphotochem

Photooxidative mineralization of microorganisms-produced glycolipid biosurfactants by a titania-mediated advanced oxidation process

Seya Ito[a], Wannasiri Worakitkanchanakul[a], Satoshi Horikoshi[a], Hideki Sakai[a,b], Dai Kitamoto[c], Tomohiro Imura[c], Sumaeth Chavadej[d], Ratana Rujiravanit[d], Masahiko Abe[a,b,*], Nick Serpone[e,**]

[a] Department of Pure and Applied Chemistry, Faculty of Science and Technology, Tokyo University of Science, 2641 Yamazaki, Noda, Chiba 278-8510, Japan
[b] Research Institute for Science and Technology, Tokyo University of Science, 2641 Yamazaki, Noda, Chiba 278-8510, Japan
[c] Research Institute for Innovations in Sustainable Chemistry, National Institute of Advanced Industrial Science and Technology (AIST), Tsukuba Central 5-2, Higashi 1-1-1, Tsukuba, Ibaraki 305-8565, Japan
[d] The Petroleum and Petrochemical College, Chulalongkorn University, Bangkok 10330, Thailand
[e] Gruppo Fotochimico, Dipartimento di Chimica Organica, Universita di Pavia, Via Taramelli 10, Pavia 27100, Italy

ARTICLE INFO

Article history:
Received 19 September 2009
Received in revised form 29 October 2009
Accepted 9 November 2009
Available online 13 November 2009

Keywords:
Glycolipid biosurfactants
Dodecylbenzene sulfonate
Titanium dioxide
Photomineralization

ABSTRACT

The photooxidative mineralizations of two microorganisms-produced glycolipid biosurfactants 4-*O*-(4′,6′-di-*O*-acetyl-2′,3′-di-*O*-alkanoyl-β-D-mannopyranosyl)-D-erythritol (MEL-A) and 1-*O*-(6′-*O*-acetyl-2′,3′-di-*O*-alkanoyl-β-D-mannopyranosyl)-D-erythritol (MEL-B) were examined by monitoring the temporal changes in UV absorption, the time profiles of CO_2 evolution and the changes in interfacial tension occurring by an advanced oxidation process in the presence of a metal-oxide (TiO_2). Features of their mineralization are compared to the photomineralization of the anionic dodecylbenzene sulfonate (DBS) surfactant carried out under otherwise identical conditions. The adsorption of surfactants on the TiO_2 surface and the positions of attack of the photogenerated •OH radicals on the surfactants' structure were assessed by molecular orbital (MO) calculations of partial charges and frontier orbital electron densities, respectively. The photodegradation of DBS was faster than the MELs as also evidenced by surface tension measurements, whereas the photomineralization of the anionic DBS surfactant was definitely slower than that of the MEL biosurfactants due to the hydrophobic alkyl chain in the DBS structure. Possible initial mechanistic stages of the photooxidation of MEL-A and MEL-B are proposed based on experimental data and comparison with MO calculations.

1. Introduction

Biosurfactants are natural surfactants produced abundantly by microorganisms from natural resources such as vegetable oils. They possess several advantages over synthetic surfactants that include, among others, mild production conditions and high environmental compatibility [1]. In general, degradation of long-lived biosurfactants is not typically examined by non-biological methods since such biosurfactants tend to be highly biodegradable. Nonetheless, to the extent that microbial degradation is too often not suitable in handling large quantities of biosurfactants it is relevant to examine alternative degradation strategies. Prompt degradation methods for biosurfactants produced by an ever increasing quantity of detergents present in ecosystems have frequently implicated advanced oxidation processes (AOPs). The photoassisted decomposition in the presence of TiO_2 represents a typical AOP technique found to be a rather strong effective oxidation method [2–4]. Studies of the decomposition of biosurfactants using AOP methods have been rather scarce.

In this article, the phoooxidative mineralization of the two microorganisms-produced glycolipid biosurfactants 4-*O*-(4′,6′-di-*O*-acetyl-2′,3′-di-*O*-alkanoyl-β-D-mannopyranosyl)-D-erythritol (MEL-A) and 1-*O*-(6′-*O*-acetyl-2′,3′-di-*O*-alkanoyl-β-D-mannopyranosyl)-D-erythritol (MEL-B), used herein as model biosurfactants, was examined in aqueous TiO_2 dispersions. The mannosyl-erythritol lipids (MELs), which represent some of the most promising glycolipid biosurfactants abundantly produced by the yeast strains of genus *Pseudozyma* [5], yield not only excellent surface and interfacial tension lowering activities but also remarkable self-assembling structures that include various lyotropic liquid crystals in aqueous media [6]. Accordingly, the present study focused on two main issues: (i) examine the mineralization of these biosurfactants in aqueous titania dispersions and compare with the concomitant mineralization of the anionic dodecylben-

* Corresponding author at: Department of Pure and Applied Chemistry, Faculty of Science and Technology, Tokyo University of Science, 2641 Yamazaki, Noda, Chiba 278-8510, Japan.
** Corresponding author. Tel.: +39 0382 98 73 16; fax: +39 0382 98 73 23.
E-mail addresses: abemasa@rs.noda.tus.ac.jp (M. Abe), nick.serpone@unipv.it, nickser@alcor.concordia.ca (N. Serpone).

1010-6030/$ – see front matter © 2009 Elsevier B.V. All rights reserved.
doi:10.1016/j.jphotochem.2009.11.007

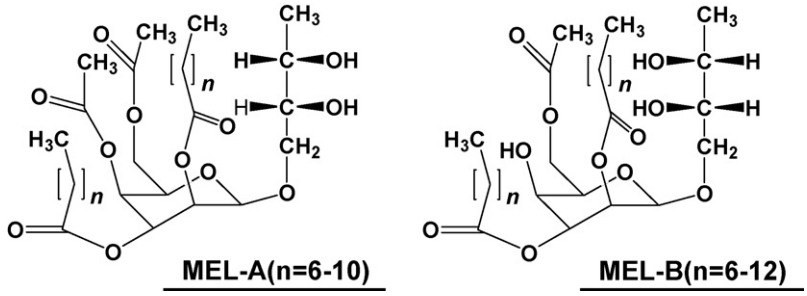

Scheme 1. Pictorial view of the two biosurfactants examined.

zene sulfonate (DBS) surfactant, examined extensively by TiO_2 AOP methods [7,8], and (ii) examine the mineralization of these MELs by considering possible initial stages of the mineralization process occurring under UV irradiation on the basis of molecular orbital calculations.

2. Experimental

2.1. Materials and reagents

The glycolipid 4-*O*-(4′,6′-di-*O*-acetyl-2′,3′-di-*O*-alkanoyl-β-D-mannopyranosyl)-D-erythritol (MEL-A) and 1-*O*-(6′-*O*-acetyl-2′,3′-di-*O*-alkanoyl-β-D-mannopyranosyl)-D-erythritol (MEL-B) (Scheme 1) were obtained by the following procedure. A seed culture (1.5 mL) of *Pseudozyma antarctica* was transferred to a 300 mL Erlenmeyer flask containing 30 mL of a fermentation medium consisting of 4% (v/v) soybean oil, $NaNO_3$ (0.2%), $MgSO_4{\cdot}7H_2O$ (0.02%), KH_2PO_4 (0.02%), yeast extract (0.1%) and water. The mixture was subsequently incubated with mixing (220 rpm) at 30 °C for 1 week. The culture broth (30 mL) was then treated twice with 30 mL of ethyl acetate. The layers were separated, and the organic layer was washed with brine and then concentrated under reduced pressure. The chloroform yellow oil solution was separated by silica gel column chromatography using a gradient mixed solvent system of chloroform/acetone (0–100%). Finally, MEL-A (>99%) was detected by its structural components containing C8 (38%), C10 (51%) and C12 (11%) fragments. The MEL-B was produced from olive oil by the *P. tsukubaensis* NBRC 1940 yeast strain and was kindly supplied by Toyobo Co. Ltd. The composition of this biosurfactant of C8 (31%), C10 (4%), C12 (32%), C14 (33%) was analyzed by gas chromatographic–mass spectrometric (GC–MS) techniques. The ratio of each alkyl chain was ascertained by matrix-assisted laser desorption/ionization time-of-flight mass spectrometry (MALDI-TOF/MS). Reagent grade sodium dodecylbenzene sulfonate (DBS) was purchased from Tokyo Kasei Kogyo Co. Titanium dioxide was Degussa P-25 (particle size, 20–30 nm by TEM observations; composition is 87% anatase and 13% rutile as determined by X-ray diffraction; surface area, 53 $m^2\,g^{-1}$ assessed by BET measurements).

2.2. Photochemical procedures

An aqueous dispersion (50 mL) consisting of the MEL biosurfactants or DBS (0.25 mM) and TiO_2 particles (50 mg) was contained in a 124-mL Pyrex vessel. The dispersion was subsequently sonicated for ca. 5 min, purged with excess oxygen gas for about 15 min, and then illuminated with a 75-W high-pressure Hg lamp (irradiation wavelengths, 365 and 334 nm; irradiance, ca. 3.0 mW cm^{-2}) under magnetic agitation.

2.3. Analytical methods and computer simulations

The photodegradation of the three surfactants was monitored by the decrease of UV absorption features at 190 nm with a Hitachi U-3310 UV–vis spectrophotometer. The temporal evolution of CO_2 (i.e., photomineralization) was monitored by gas chromatography using a Shimadzu GC-2014 chromatograph with TCD detection and a Porapack Q column; helium was the carrier gas. The interfacial tension (water/decane) of aqueous MEL-A, MEL-B and DBS solutions was determined by the pendant drop method at 25 °C using an apparatus that consisted of an automatic interfacial tensiometer (DM500, Kyowa Interface Science, Japan) and a FAMAS version 2.01 Drop Shape Analysis Software.

Molecular orbital calculations were carried out at the single determinant (Hartree–Fock) level for optimization bearing the minimum energy obtained at the AM1 level [9]. All semi-empirical calculations were performed in MOPAC version 6.2 with a CAChe package (Fujitsu Co. Ltd.). An initial position of •OH radical attack was estimated from the calculation of frontier orbital electron densities (FOEDs). The adsorption behaviors of the surfactants on the TiO_2 surface were inferred by the calculated point charges [10,11].

2.4. Inference of biodegradability of MEL-A, MEL-B and DBS surfactants

The biochemical oxygen demand (BOD; determined over a 10-day period) and total organic carbon (TOC) for the MEL-A, MEL-B biosurfactants and the DBS substrate with initial concentrations 50 mg L^{-1} were measured using a Japan Industrial Standard (JIS K0102-21) and a Shimadzu TOC-5000 analyzer, respectively. The relevant data are reported in Table 1.

3. Results and discussion

Time profiles of the concentration changes from the UV absorption features during the photoassisted degradation of MEL-A, MEL-B and DBS surfactants are illustrated in Fig. 1a. The initial adsorption of DBS on the TiO_2 surface under dark conditions was ca. 8.3%. In the case of the MEL surfactants (initial concentration also 0.25 mM), the initial adsorption in the dark on the TiO_2 surface was more extensive at 68% for MEL-A and 92% for MEL-B. Evidently, there exists a structural feature on these two biosurfactants, likely the pyrano ring that facilitates their adsorption on the metal-oxide surface. The

Table 1
Biochemical oxygen demand (BOD) and total organic carbon (TOC) for the MEL-A, MEL-B and DBS (50 mg L^{-1}) surfactants.

Substrates	BOD (mg L^{-1})	TOC (mg L^{-1})
MEL-A	28.0	29.9
MEL-B	22.3	31.0
DBS	19.4	31.0

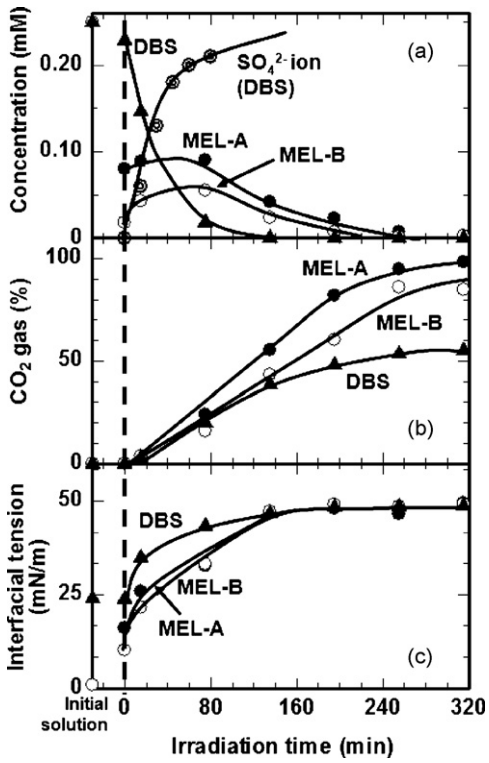

Fig. 1. (a) Temporal decrease of the concentration of MEL-A, MEL-B and DBS, and increase of SO_4^{2-} concentration for DBS; (b) evolution of CO_2 gas and (c) increase of the interfacial tension in the photodecomposition of MEL-A, MEL-B and DBS (initial concentrations, 0.25 mM) in TiO_2 dispersions (50 mg) under UV illumination.

UV absorption of the MEL surfactants decreased with UV irradiation time beyond the first 80 min of illumination. In the first 80 min, the MEL concentrations appeared to increase with irradiation, which we attribute to photodesorption of the biosurfactants since there were no positional changes of the spectral patterns. For the DBS surfactant the photomineralization progressed through first-order kinetics with 99% of the benzene ring band disappearing completely after ca. 130 min. Both the MEL-A and MEL-B systems degraded by otherwise identical first-order rates $\{k_{deg} = (1.3 \pm 0.1) \times 10^{-2}\ min^{-1}$ and $(1.5 \pm 0.1) \times 10^{-2}\ min^{-1}$, respectively$\}$. By comparison the rate for the DBS surfactant was about twofold faster $\{k_{deg} = (3.1 \pm 0.1) \times 10^{-2}\ min^{-1}\}$ and formation of sulfate ions (desulfonation) was $k_{sulf} = (2.3 \pm 0.5) \times 10^{-2}\ min^{-1}$ both of which we attribute to a faster attachment of the •OH radicals to the phenyl ring of DBS relative to H-abstraction in the MEL structures (Scheme 1). In the latter case of DBS, the extent of degradation occurs in parallel with desulfonation (see Fig. 1a).

The temporal evolutions of CO_2 emanating from the photomineralization of the MEL-A, MEL-B and DBS substrates are depicted in Fig. 1b. The quantities of CO_2 evolved were 24% (MEL-A) ≥ 20% (DBS) ≥ 16% (MEL-B) for a 75-min UV illumination period. At longer irradiation time (ca. 255 min) the quantities of CO_2 evolved were MEL-A (95%) > MEL-B (86%) ≫ DBS (54%). For the latter surfactant (DBS), the initial stage of photodegradation involved the evolution of CO_2 from the photomineralization of the benzene ring carbons, whereas the later stage involved the slower photomineralization of the alkyl group carbons. By contrast, CO_2 gas evolution was rather constant for the MEL-A surfactant compared to the DBS case, probably owing to the extensive adsorption of this biosurfactant onto the TiO_2 particle surface. This is the major difference between the MEL surfactants and DBS. Regardless, the dynamics of evolution of carbon dioxide were $k(CO_2) = (7.1 \pm 1.0) \times 10^{-3}\ min^{-1}$ for MEL-A, $(5.0 \pm 0.6) \times 10^{-3}\ min^{-1}$ for MEL-B and $(3.0 \pm 0.2) \times 10^{-3}\ min^{-1}$ for DBS.

The increases in the interfacial tension that accompanied the photoassisted degradation and mineralization of MEL-A, MEL-B and DBS solutions are displayed in Fig. 1c. The critical aggregation concentrations (CAC) of the surfactants are 0.0040 mM (MEL-A), 0.010 mM (MEL-B) and 0.18 mM (DBS). The initial interfacial tensions of the surfactants (0.25 mM) were 0.9 mN m^{-1} (MEL-A),

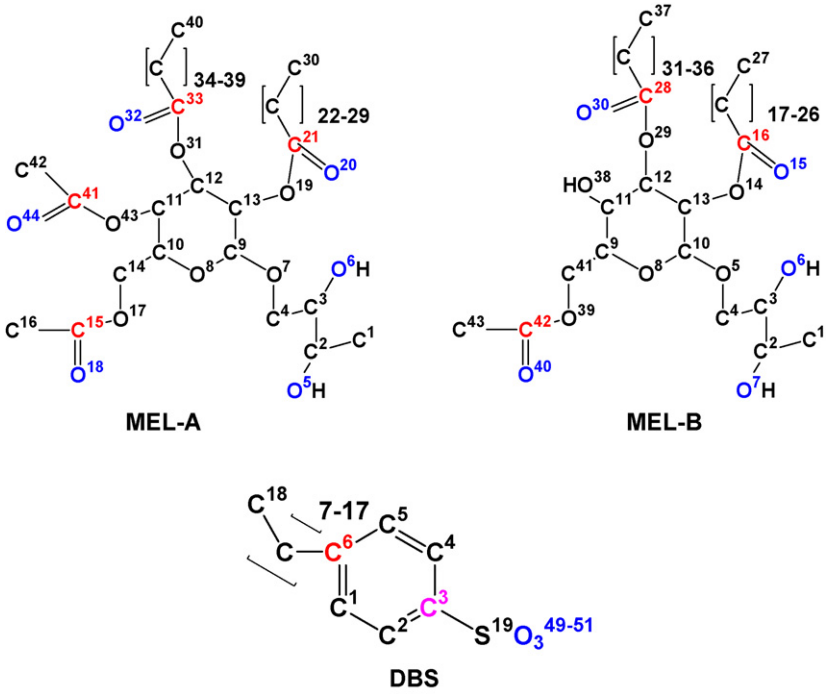

Fig. 2. Structures of the surfactants and the numbering scheme used in the MO calculations of point charges and frontier orbital electron densities. Atoms colored blue are those with the greatest negative charge whereas those colored red are the atoms with the greatest frontier orbital electron densities. The C3 atom in DBS bore both a large negative charge and a high electron density. (For interpretation of the references to color in this figure and Table 2 data, the reader is referred to the web version of the article.)

0.9 mN m^{-1} (MEL-B) and 24 mN m^{-1} (DBS). The interfacial tensions of the MEL solutions increased with addition of TiO_2 particles under dark conditions, likely due to a decrease in the MEL concentrations in solution subsequent to adsorption of the MEL biosurfactants on the TiO_2 surface. By contrast, no change in the interfacial tension of DBS occurred on addition of TiO_2 particles, in line with the small extent of adsorption of DBS on the metal-oxide surface. After 135 min of UV irradiation the interfacial tension increased to ca. 47 mN m^{-1} for MEL-A, MEL-B and DBS approaching that of water (ca. 50 mN m^{-1}) on further UV irradiation. The time profiles of interfacial tension for the surfactants do not correlate with the tendency of CO_2 evolution. The increase of the interfacial tension for DBS was faster than for the MEL surfactants, whereas evolution of CO_2 gas was slowest for DBS. That is, the photomineralization of the hydrophobic groups in the DBS structure was remarkably slow compared with the photomineralization of the hydrophilic groups. On the other hand, the photomineralization of the hydrophilic and hydrophobic groups in the MEL structures occurred concomitantly at the TiO_2/water interface.

Analysis of the initial adsorption on the TiO_2 surface and of the photoactive site at which chemistry begins with respect to the chemical structure was not facilitated by the relatively fast photoreactions. The surface of the TiO_2 particles is positively charged in aqueous media at pHs below 6.3, changing from a = Ti–OH neutral surface to a = Ti–OH_2^+ positively charged surface. The pH of each solution was ca. 6.0. Accordingly, the functions in the structures bearing the greatest negative charge are expected to lie closest to the positively charged TiO_2 surface. The reactions were initiated by •OH radicals produced at the TiO_2/OH^- (H_2O) interface by the positive holes (h^+) after adsorption of the surfactants on the TiO_2 surface. Attack of the •OH radicals occurred at the function(s) bearing the highest frontier orbital electron densities (FOED) of the surfactant that were estimated using the MOPAC software package. Turchi and Ollis [12] have pointed out that the average distance of diffusion of the hydroxyl radicals from the TiO_2 surface depends on the concentration of the substrates and the rates of reaction between the •OH radicals and the substrates. However, the •OH radical can only distance itself from the TiO_2 surface a short distance of no more than a few nm (i.e. a few 10 Å), if at all [13]. As such, •OH radical attack of the surfactant's components will likely occur at the TiO_2 surface, so that a function of the surfactant containing the richest frontier orbital electron density near the surface of TiO_2 will be attacked preferentially. Therefore, as the distance between a negatively charged atom and an atom having a higher FOED is shortened, the rates of photodegradation and mineralization are expected to increase. Details of the estimated adsorption of some surfactants on

Table 2
Point charges (PC) and frontier orbital electron densities (FOEDs) for MEL-A, MEL-B and DBS molecules using semi-empirical molecular orbital (MO) calculations (H atoms were included in calculations but are not reported herein).

MEL-A[a]			MEL-B			DBS		
Atom	PC	FOEDs	Atom	PC	FOEDs	Atom	PC	FOEDs
C1	–0.258	0.010	C1	–0.235	0.003	C1	–0.187	0.235
C2	0.039	0.015	C2	0.038	0.015	C2	–0.033	0.253
C3	0.025	0.016	C3	–0.004	0.021	**C3**	**–0.876**	**0.365**
C4	–0.065	0.017	C4	–0.061	0.015	C4	–0.013	0.265
O5	**–0.411**	0.033	O5	–0.300	0.027	C5	–0.187	0.219
O6	**–0.378**	0.028	**O6**	**–0.398**	0.021	**C6**	0.002	**0.393**
O7	–0.304	0.024	**O7**	**–0.406**	0.028	C7	–0.150	0.028
O8	–0.320	0.036	O8	–0.316	0.032	C8	–0.162	0.006
C9	0.141	0.017	C9	0.146	0.017	C9	–0.161	0.005
C10	0.013	0.014	C10	0.025	0.012	C10	–0.161	0.006
C11	–0.007	0.026	C11	0.003	0.017	C11	–0.160	0.006
C12	0.014	0.023	C12	–0.024	0.028	C12	–0.160	0.007
C13	–0.003	0.028	C13	–0.004	0.028	C13	–0.160	0.007
C14	–0.019	0.008	O14	–0.283	0.034	C14	–0.160	0.007
C15	0.393	**0.091**	**O15**	**–0.452**	0.074	C15	–0.160	0.006
C16	–0.241	0.003	**C16**	0.372	**0.191**	C16	–0.160	0.006
O17	–0.298	0.016	C17	–0.174	0.012	C17	–0.162	0.005
O18	**–0.496**	0.036	C18	–0.160	0.013	C18	–0.223	0.002
O19	–0.283	0.033	C19	–0.161	0.018	S19	3.029	0.030
O20	**–0.448**	0.070	C20	–0.161	0.024	**O49**	**–1.175**	0.012
C21	0.367	**0.181**	C21	–0.160	0.027	**O50**	**–1.156**	0.007
C30	–0.223	0.012	**O30**	**–0.446**	0.102			
O31	–0.288	0.027	C31	–0.173	0.013			
O32	**–0.452**	0.057	C32	–0.161	0.020			
C33	0.375	**0.140**	C33	–0.161	0.017			
C40	–0.223	0.011	**O40**	**–0.494**	0.046			
C41	0.380	**0.154**	C41	–0.049	0.012			
C42	–0.241	0.005	**C42**	0.388	**0.119**			
O43	–0.283	0.029	C43	–0.240	0.003			
O44	**–0.470**	0.057						

[a]Partial charges for the C22–C29 methylene carbons of MEL-A ranged from −0.173 to −0.160, whereas for the methylene C34–C39 carbons they ranged from −0.172 to −0.160. The frontier orbital electron densities for these carbons ranged from 0.012 to 0.031 and from 0.011 to 0.028, respectively.

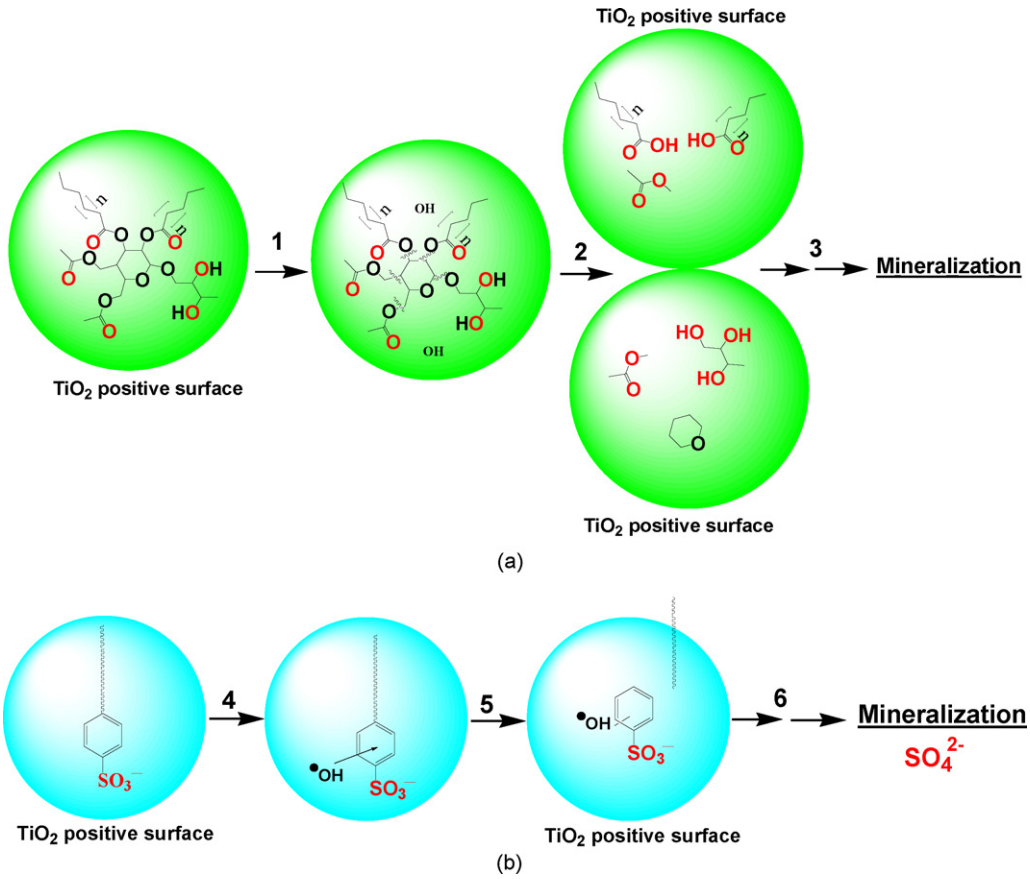

Scheme 2. (a) Proposed initial stages in the photomineralizations of the MEL biosurfactants on the TiO_2 surface. (b) Proposed initial degradation mechanism of the DBS surfactant on the TiO_2 surface.

the TiO_2 surface and the positions of •OH radical attack on the surfactant structures by molecular orbital simulations were reported earlier [10].

Fig. 2 illustrates the structures of the surfactants and the numbering scheme used in the MO calculations of the point charges and the frontier orbital electron densities. The oxygen atoms colored blue are those with the greatest negative charge (range: −0.378 to −0.496 for MEL-A and −0.398 to −0.484 for MEL-B; Table 2), whereas the carbon atoms colored red are the atoms with the greatest FOEDs (range: 0.091–0.181 for MEL-A and 0.119–0.264 for MEL-B). The C3 carbon atom in DBS bore both a large negative point charge (−0.876) and a FOED of 0.365, with the C6 carbon bearing a slightly greater electron density (0.393); the oxygen atoms of the sulfonate group possessed the greatest negative point charges (−1.156 to −1.175).

The atoms having the most negative charge in MEL-A and MEL-B are the oxygen atoms. Averaged partial point charges of all the oxygen atoms in the MEL-A were 6-fold greater (negatively) than the charges on the carbon atoms. The MEL-B biosurfactant showed a similar tendency. Accordingly, the oxygen atoms in the MEL structures are the positions of closest approach of the biosurfactants to the TiO_2 metal-oxide surface and thus the most likely sites of adsorption (step 1 in Scheme 2a). The highest frontier orbital electron densities in the MEL-A and MEL-B structures are the carbonyl carbons that are therefore highly susceptible to attack by the •OH radicals (step 2), following which cleavage of the pyrano ring and further oxidation of the intermediates (steps 3) of the MEL molecules would occur leading ultimately to mineralization with more than 80% yield of carbon dioxide produced (Fig. 1b) from the biosurfactant substrates.

For DBS, the anionic sulfonate moiety ($-SO_3^-$) is the only site of adsorption of this surfactant onto the positively charged TiO_2 surface (Scheme 2b). The richest frontier orbital electron density is concentrated on the C–alkyl and C–SO_3^- bonds of the aromatic ring (step 4). Therefore, if the initial degradation of DBS occurred through partial cleavage at the C–SO_3^- site the compounds resulting from the surfactant decomposition would have hydrophobic properties and exhibit no surface activity (step 5). The interfacial tension increased with irradiation time (see Fig. 1c). However, mineralization of DBS tended to slow down achieving only about 50% yield of carbon dioxide (Fig. 1b) after ca. 4 h of irradiation from the phenyl carbons. The hydrophobic alkyl chain is more resistant to photooxidation as it does not adsorb well on the metal-oxide surface. In summary, the difference(s) in the photodegradation of DBS and MEL surfactants must be seen as originating mostly from differences in the mode of adsorption of the substrates on the TiO_2 surface.

4. Concluding remarks

In the initial stages the MEL biosurfactants are strongly adsorbed on the TiO_2 surface in aqueous dispersions through the various hydrophilic groups (i.e. oxygen atoms) present in the MEL structures, subsequent to which photodegradation/mineralization progresses fairly rapidly by attack of •OH radicals onto the atoms bearing the larger electron densities of the hydrophilic (and then hydrophobic) functions. The only site of adsorption for the DBS surfactant on the positively charged TiO_2 surface is the sulfonate group. In the latter case, •OH radical attack focused mostly on the benzene ring bearing the highest electron density in the

DBS structure, particularly at the C3 and C6 carbons, leading to cleavage of the alkyl chain away from the TiO_2 surface. The consequent photomineralization of the released alkyl chain proved to occur slowly. Generally, the photoassisted mineralization of hydrophobic groups tends to be remarkably slower compared to hydrophilic groups [8]. Related to the present study on the MEL biosurfactants, the nonylphenol ethoxylate systems (NPEs) that are discharged into aquatic ecosystems (e.g. rivers) are typically biodegraded through bacterial attack of the ethoxyl moieties to yield the hydrophobic/hydrophilic intermediate nonylphenol (NP) [14–16], a toxic substance (an endocrine disruptor) which tends to persist in nature. In the presence of TiO_2, the NPEs are mineralized with greater efficiency than are typical cationic and anionic surfactants; nonetheless, a mineralization yield of 75% was obtained for NPEs only after 8 h of irradiation [17]. Near-quantitative mineralization of the MEL biosurfactants was achieved herein after about 4 hrs of irradiation under conditions similar to those used earlier for NPEs [17]. The present study has shown that biodegradable surfactants (MELs) can also be treated in relatively short time by advanced oxidation processes involving the metal-oxide (TiO_2).

Acknowledgments

We are grateful to the personnel of the water treatment company Nippon Filter Co. Ltd. for assistance in measuring the biochemical oxygen demand for the surfactants examined in this study and the staff at Fujitsu Co. Ltd. for discussions on the MOPAC calculations. NS is grateful to Prof. Abe for a Visiting Professorship at the Tokyo University of Science for the period July–August, 2008.

References

[1] D. Kitamoto, H. Isoda, T. Nakahara, Functions and potential applications of glycolipid biosurfactants—from energy-saving materials to gene delivery carriers, J. Biosci. Bioeng. 94 (2002) 187–201.
[2] O. Legrini, E. Oliveros, A.M. Braun, Photochemical processes for water treatment, Chem. Rev. 93 (1993) 671–698.
[3] A. Mills, R.H. Davies, D. Worsley, Water purification by semiconductor photocatalysis, Chem. Soc. Rev. 22 (1993) 417–425.
[4] M.A. Fox, M.I. Dulay, Heterogeneous photocatalysis, Chem. Rev. 93 (1993) 341–357.
[5] T. Morita, M. Konishi, T. Fukuoka, T. Imura, H.K. Kitamoto, D. Kitamoto, Characterization of the genus *Pseudozyma* by the formation of glycolipid biosurfactants, mannosylerythritol lipids, FEMS Yeast Res. 7 (2007) 286–292.
[6] D. Kitamoto, H. Yanagishita, T. Shinbo, T. Nakane, C. Kamisawa, T. Nakahara, Surface active properties and antimicrobial activities of mannosylerythritol lipids as biosurfactants produced by *Candida antarctica*, J. Biotechnol. 29 (1993) 91–96.
[7] H. Hidaka, J. Zhao, E. Pelizzetti, N. Serpone, Photodegradation of surfactants. 8. Comparison of photocatalytic processes between anionic DBS and cationic BDDAC on the titania surface, J. Phys. Chem. 96 (1992) 2226–2230.
[8] H. Hidaka, S. Horikoshi, J. Zhao, Photodegradation of surfactants in UV-illuminated aqueous TiO_2 dispersions, J. Oleo Sci. 1 (2001) 55–73.
[9] M.J.S. Dewar, E.G. Zoebisch, E.F. Healy, J.J.P. Stewart, Development and use of quantum mechanical molecular models. 76. AM1: a new general purpose quantum mechanical molecular model, J. Am. Chem. Soc. 107 (1985) 3902–3909.
[10] S. Horikoshi, N. Serpone, S. Yoshizawa, J. Knowland, H. Hidaka, Photocatalyzed degradation of polymers in aqueous semiconductor suspensions: IV. Theoretical and experimental examination of the photooxidative mineralization of constituent bases in nucleic acids at titania/water interfaces, J. Photochem. Photobiol. A: Chem. 120 (1999) 63–74.
[11] S. Horikoshi, H. Hidaka, Photodegradation mechanism of heterocyclic two-nitrogen containing compounds in aqueous TiO_2 dispersions by computer simulation, J. Photochem. Photobiol. A: Chem. 141 (2001) 201–208.
[12] C.S. Turchi, D.F. Ollis, Photocatalytic degradation of organic water contaminants: mechanisms involving hydroxyl radical attack, J. Catal. 122 (1990) 178–192.
[13] (a) D. Lawless, N. Serpone, D. Meisel, A semiconductor photophysics. 6. The role of OH radicals and trapped holes in photocatalysis. A pulse radiolysis study, J. Phys. Chem. 95 (1991) 5166–5170;
(b) N. Serpone, D. Lawless, R. Terzian, D. Meisel, A redox mechanisms in heterogeneous photocatalysis. The case of holes vs. OH radical oxidation and free vs. surface-bound OH radical oxidation processes, in: R. McKay, J. Texter (Eds.), Electrochemistry in Colloids and Dispersions, VCH Publishers, New York, 1992, pp. 399–416.
[14] L. Rudling, P. Solyom, The investigation of biodegradability of branched nonylphenol ethoxylates, Water Res. 8 (1974) 115–119.
[15] W. Giger, E. Stephanou, C. Schaffer, Persistent organic chemicals in sewage effluents: I. Identifications of nonylphenols and nonylphenolethoxylates by glass capillary gas chromatography/mass spectrometry, Chemosphere 10 (1981) 1253–1263.
[16] E. Stephanou, W. Giger, Persistent organic chemicals in sewage effluents. 2. Quantitative determinations of nonylphenols and nonylphenol ethoxylates by glass capillary gas chromatography, Environ. Sci. Technol. 16 (1982) 800–805.
[17] S. Horikoshi, N. Watanabe, H. Hidaka, Photocatalytic wastewater treatment for 4-nonylphenol of an endocrine disruptor and 4-nonylphenol polyethoxylate surfactants at the titania/water interface, J. Jpn. Oil Chem. Soc. 49 (2000) 631–639.